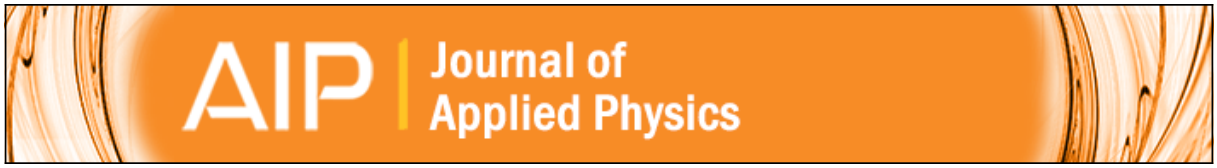

Optical transition in infrared photodetector based on V-groove Al 0.5 Ga 0.5 As/GaAs multiple quantum wire

Y. Fu, M. Willander, X.-Q. Liu, W. Lu, S. C. Shen, H. H. Tan, C. Jagadish, J. Zou, and D. J. H. Cockayne

Citation: Journal of Applied Physics **89**, 2351 (2001); doi: 10.1063/1.1339857

View online: http://dx.doi.org/10.1063/1.1339857

View Table of Contents: http://scitation.aip.org/content/aip/journal/jap/89/4?ver=pdfcov

Published by the AIP Publishing

Optical transition in infrared photodetector based on V-groove $Al_{0.5}Ga_{0.5}As/GaAs$ multiple quantum wire

Y. Fu[a] and M. Willander
Physical Electronics and Photonics, MC2, Department of Physics, Fysikgränd 3, University of Gothenburg and Chalmers University of Technology, S-412 96 Gothenburg, Sweden

X.-Q. Liu, W. Lu, and S. C. Shen
National Laboratory for Infrared Physics, Shanghai Institute of Technical Physics, Chinese Academy of Science, Shanghai 200083

H. H. Tan and C. Jagadish
Department of Electronic Material Engineering, Research School of Physical Science and Engineering, the Australian National University, Canberra 0200, A.C.T., Australia

J. Zou and D. J. H. Cockayne
Australian Key Center for Microscopy and Microanalysis, The University of Sydney, NSW 2006, Australia

(Received 6 March 2000; accepted for publication 15 November 2000)

Photoconductors based on V-grooved $Al_{0.5}Ga_{0.5}As/GaAs$ multiple quantum wires (QWR) were fabricated. The geometric structure of the QWR was carefully characterized by transmission electron microscopy and spatially resolved microphotoluminescence measurements. Infrared response at 9.2 μm is observed from the photocurrent spectrum measured at 80 K. It is attributed as the intersubband transition in the quantum wire region. Due to the effective quantum confinement from the two (111)-surfaces forming the V groove, the overlapping between the ground state in the QWR and the one in the vertical quantum well is very small. This explains the weak photocurrent signal from the QWR photodetector. Theoretical design for a better wave function overlapping and optical coupling is outlined from the analysis of two-dimensional spatial distributions of the wave functions. © *2001 American Institute of Physics.* [DOI: 10.1063/1.1339857]

I. INTRODUCTION

Nanostructure growth techniques and low-dimensional system fabrications have been undertaking considerable research and development effort as a consequence of their promising technological applications. From the pioneer work of Esaki and Tsu,[1] semiconductor quantum well (one-dimensional quantum confinement) has been a constant interest in electronics and optoelectronics, both in the research laboratories and in the industries.[2–5] Electronic and optical studies on quantum wires (two-dimensional quantum confinement) were started by Sakaki[6] at the beginning of 1980s. It has been expected that the additional quantum confinement of the carriers can lead to significant improvement in device performance.[7] Quantum wire lasers exhibit much narrower and higher peak gain values as compared with quantum well lasers.[8–10] In addition to the optoelectronics applications, quantum-wire-based field effect transistor[11] and resonant tunneling[12] were also reported. Various semiconductor materials have been exploited, e.g., GaAlAs/GaAs,[13,14] InGaAs/GaAs,[15,16] ZnCdSe/ZnSe,[17,18] and even $Si_{1-x}Ge_x$-based samples.[19]

Theoretical analysis of the system remains a nontrivial task due to the complication in solving the multiple-dimensional Schrödinger equation. Considerable effort has been put forth to calculate the energy sublevels and wave functions, e.g., local-envelop state expansion,[20] plane-wave expansion,[21] finite-element method,[22] and effective potential calculation.[23] Difficult as the eignvalue and eigenfunction problem, it must be treated for the material/device characterization and design.

In this article, we report the growth and characterization of an infrared photodetector based on the GaAs/AlGaAs multiple-quantum wire (QWR) structure on V-grooved substrate in Sec. II. The theoretical analysis about the optical transition in QWR is presented in Sec. III based on the Green's function theory (for eigenvalues of the model Hamiltonian) and the finite element method (for eigenfunctions).

II. EXPERIMENT

Semi-insulating GaAs (100) substrate was processed by standard photolithography and wet etching. Fifty V grooves (each 2 μm wide) were arranged periodically with a 2 μm spacing along the *y* direction. A 0.1-μm-thick GaAs buffer layer was grown before the 1-μm-thick $Al_{0.5}Ga_{0.5}As$ layer. Both layers were Si doped at a level of 10^{18} cm^{-3} as the lower contact layer. Twenty periods of nominal 75-nm-thick $Al_{0.5}Ga_{0.5}As$ undoped barrier and 3-nm-thick Si doped (10^{18} cm^{-3}) GaAs well layers were grown along the *z* direction as the active optical absorption layer. The structure was terminated by a 0.2-μm-thick Si-doped (10^{18} cm^{-3}) GaAs top contact layer.

[a]Electronic mail: fyg@fy.chalmers.se

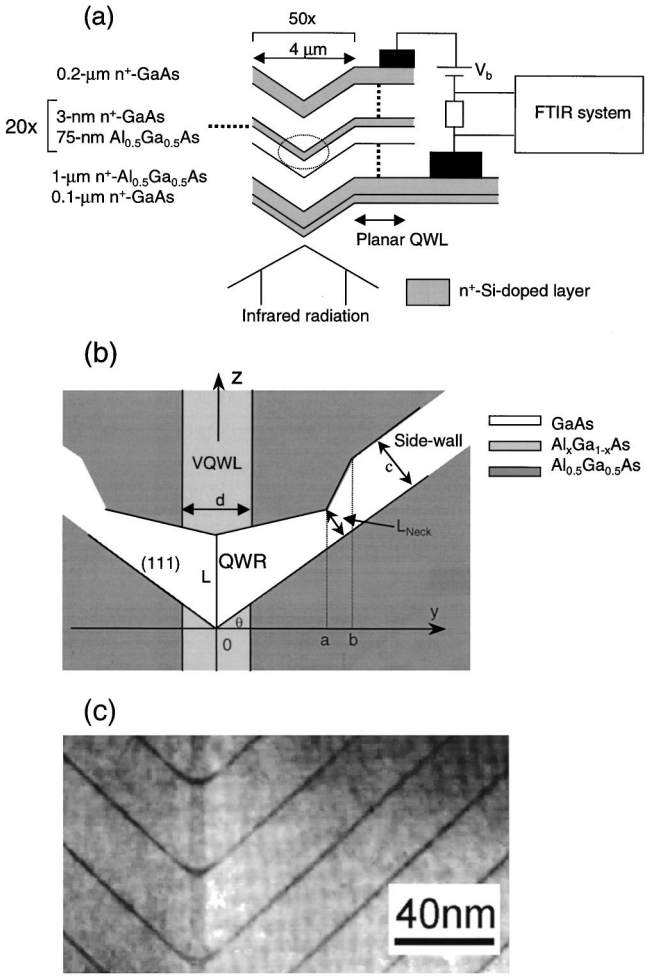

FIG. 1. (a) Schematic structure of the QWR infrared photoconductor. (b) Geometric structure of the quantum wire. $L=9.5\pm1.5$, $c=4.5\pm1.5$, $a=20$, $b=28$, $L_{\text{neck}}=1.4$, $d=12.8\pm1.5$ nm determined from the TEM image of the sample cross section. $\theta=35.5°$ for the (111)-substrate. (c) TEM image of the cross section.

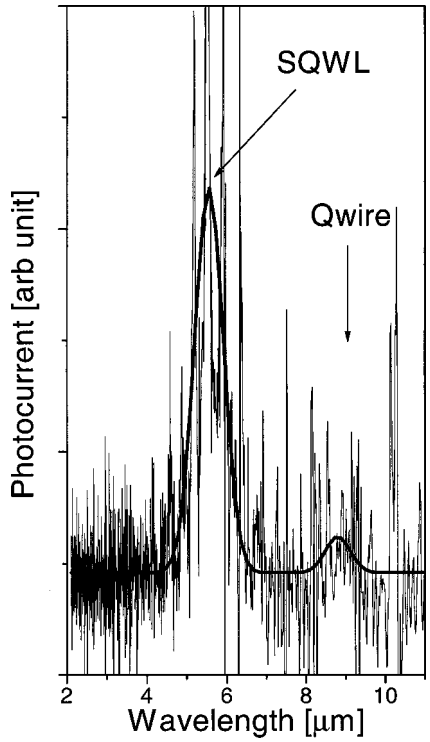

FIG. 2. Photocurrent spectrum at an external bias of 6 V. Sample temperature is about 80 K.

Photodetector mesas having a surface area of 200×200 μm^2 were fabricated on the 50 V grooves. AuGeNi/Au alloy was deposited and metallized as the electrode contact. The photodetector is schematically shown in Fig. 1(a) and the detailed cross section of the QWR sample in Fig. 1(b) based on the transmission electron microscopy (TEM) [Fig. 1(c)].

The sample photodetector was then loaded in the cryostat and cooled down with liquid N_2. Infrared radiation was introduced normal to the sample surface and the photocurrent was measured by a Bruker 113 Fourier transform spectrometer. Figure 2 shows the photocurrent spectrum at an external bias of 6 V. Two response peaks, 5.5 and 9.0 μm were observed (the bold curve is obtained by multiple-peaks Gaussian fitting).

As demonstrated by Fig. 1, several different quantum confinement structures exist in the QWR photodetector. Most important are the sidewall quantum well (SQWL), the vertical quantum well (VQWL) and the planar quantum well (PQWL) (included in the device mesa).

In order to characterize the geometric structure of the system, microphotoluminescence spectra of the QWR samples at room temperature were measured by high spatial resolution Dilor-super-infinity analytic micro-Raman system (the 514.5 nm line from an Ar+ laser was used as the excitation source with a spot diameter of less than 1 μm).[24] Together with the transmission electron microscopy of Fig. 1(c) we are able to construct the detailed geometric structure of our QWR sample by comparing the excitation energies (obtained from the local densities of states by the Green's function.[25]) The results are $L=8.0$, $c=3.2$, $a=20.0$, $b=28.0$, $L_{\text{neck}}=1.4$, $d=12.0$ nm. An Al mole fraction of 0.2125 at the VQWL has also been deduced.

Knowing the geometric structure of the system it is easy to obtain numerically that in the PQWL and SQWL spatial regions the energy differences between the ground electron states and the first excited state are 227 and 217 meV, respectively. These values correspond to optical responses at 5.5 and 5.7 μm, which are believed to contribute to the measured photocurrent peak at 5.5 μm. On the other hand, the ground electron state in the VQWL is 197.7 meV and the one in the QWR is at 66.38 meV. Energy separation between these two states is 131.3 meV (9.4 μm), which is very close to the 9.0 μm peak observed in the photocurrent spectrum.

III. OPTICAL TRANSITION BETWEEN GROUND STATES IN QWR AND VQWL

We concentrate on the optical transition in the QWR region. Optical radiation excites electrons occupying the ground state in the QWR to the states which are continuous along the VQWL region (z axis). These carriers are then driven by the external bias to form the photocurrent. The photocurrent could be weak as compared with the one originated from the SQWL and PQWL regions because of the

much limited spatial area of the QWR region. In the yz plane (Fig. 1), it is the size comparison between a dot (QWR) with a line (SQWL/PQWL). However, since the ground states in SQWL and PQWL regions are about 0.1682 eV which are much higher than the one in the QWR region (0.066 eV), we expect higher carrier concentration in the QWR region at low temperature (liquid N_2 temperature for normal device application). Therefore, a detailed quantitative analysis is of necessity.

Theoretically the $Al_{0.5}Ga_{0.5}As$ system is an indirect band gap material where $\Gamma-X$ mixing effect in the conduction band can be important.[26] However, the characteristics of the photoluminescence spectrum is determined by the interband transitions between ground electronic and ground hole states in various spatial regions. Optical transition of interest is between the ground sublevel in the QWR region and the band edge of the continuous states in the VQWL. These ground states are far below the barrier heights (both Γ and X bands) so that they are hardly affected by the $\Gamma-X$ mixings. We therefore consider only the Γ electron and apply the effective mass theory to describe the QWR photodetector in the two-dimensional yz plane. The effective mass of the Γ electron is 0.067 in the unit of free electron mass and the conduction band offset between $Al_xGa_{1-x}As$ and GaAs is $0.65\times 1.247x$ eV.

We consider optical transitions between sublevels in the quantum wire system of Fig. 1. We have defined the growth direction as the z axis. The 50 quantum wires are placed periodically along the y direction and are aligned along the x axis. The two-dimensional Hamiltonian of the system is expressed as

$$-\frac{\hbar^2}{2m^*}\frac{\partial^2}{\partial y^2}-\frac{\hbar^2}{2m^*}\frac{\partial^2}{\partial z^2}+V(y,z) \tag{1}$$

in the effective mass approximation. The total wave function of the sublevel can be expressed as

$$\Psi_{n,k}(\boldsymbol{r})=\psi_n(y,z)e^{ikx}u(\boldsymbol{r}), \tag{2}$$

where e^{ikx} accounts the translational symmetry along the x axis and $u(\boldsymbol{r})$ is the conduction band Bloch function. $\psi_n(y,z)$ is the envelop function of the nth sublevel in the quantum wire region.

Our numerical analysis of the two-dimensional system starts with the Green's function theory for the eigenvalues. Knowing the eigenvalues, the Schrödinger equation is solved by the standard finite element method for the eigenfunctions. Calculated energy band structure (local density of states from local Green's function) is presented in Fig. 3(a) where we observe three localized states in the QWR region below the ground state of the VQWL which is extended in the z direction. The local density of states (LDOS) of the VQWL far away from the QWR region is presented as the dotted line. It is noticed that the whole system is extended along the x direction and the local densities of states presented in Fig. 3 correspond to a two- dimensional Hamiltonian of Eq. (1).

The ground state in the QWR locates at 66.38 meV (we take the conduction band edge of GaAs as the reference energy). Energy separation between this state and the ground state in the VQWL is 131.3 meV (9.4 μm), which is reasonably close to the 9.2 μm peak observed in the photocurrent spectrum. Optical excitations are also possible among the three confined electron states in the QWR region. However, the corresponding photocurrent is much limited as compared with the free transport of the carriers occupying extended states in the VQWL along the z direction.

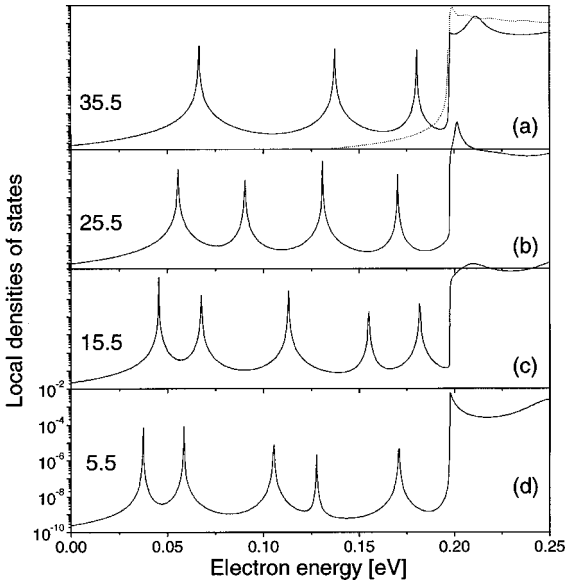

FIG. 3. Electron local densities of states of the QWR system. Dotted line: LDOS of VQWL. (a) $\theta=35.5°$; (b) $\theta=25.5°$; (c) $\theta=15.5°$; (d) $\theta=5.5°$.

The spatial distribution of the ground state, $\Psi_0(y,z)$ is plotted in Fig. 4(a). It is found that the quantum confinement from the two (111) surfaces [having a spatial angle of $\theta=35.5°$ in Fig. 1(b)], forming the V groove, is so effective that the wave function is significant along the z-axis. Its extension in the y direction is only about 4 nm. Elsewhere it decays exponentially. Artificially reducing the quantum confinement by reducing θ (increasing the angle between two confinement surfaces), the spatial distribution of the ground state in the QWR region expands rapidly, as demonstrated by Figs. 4(b) and 4(c). The energy position of the ground state is lowered by an amount of 20 meV (Figs. 3 and 4) when decreasing θ from 35.5° to 15.5°.

The ground state in the VQWL extends periodically along the z direction with a period of 78 nm (3 nm GaAs plus 75 nm $Al_{0.5}Ga_{0.5}As$). It decays exponentially when $|y|>d/2$, here $d=12$ nm. The two-dimensional wave function is contour plotted in Fig. 5(a) in the region where the ground state in the QWR is significant. We have plotted the profile of the QWR together with the vertical line of $y=d/2$ in Figs. 3 and 4 for calibration.

Knowing the eigenvalues and eigenfunctions describing the active electrons, the interaction between the incident radiation and the electron in the system is

$$\frac{e}{m^*}\boldsymbol{A}\cdot\boldsymbol{p}=\frac{e}{m^*}(A_xp_x+A_yp_y) \tag{3}$$

for the present device configuration where the radiation propagates along the z direction

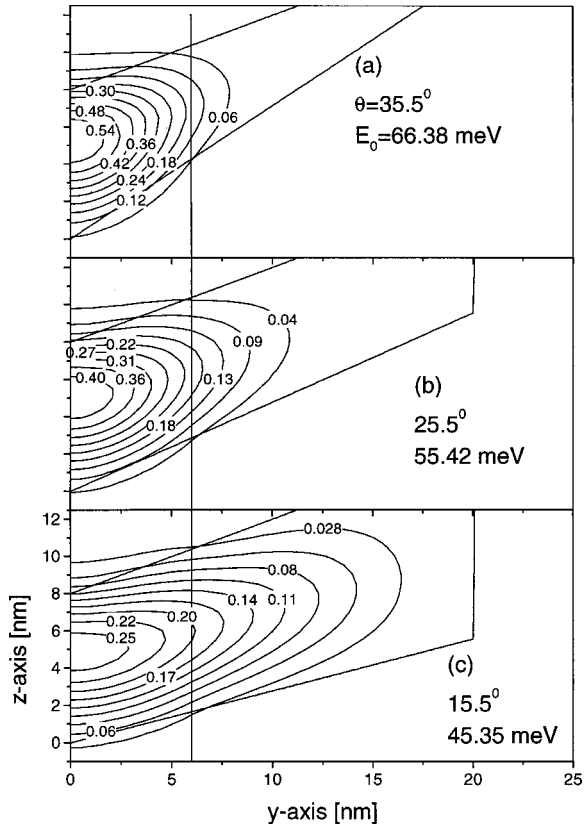

FIG. 4. Spatial distribution (contour plot) of the ground state in the QWR region. (a) $\theta=35.5°$, $E_0=66.38$ meV; (b) $\theta=25.5°$, $E_0=55.42$ meV; (c) $\theta=15.5°$, $E_0=45.35$ meV. Straight lines: profiles of various V-grooved quantum wires.

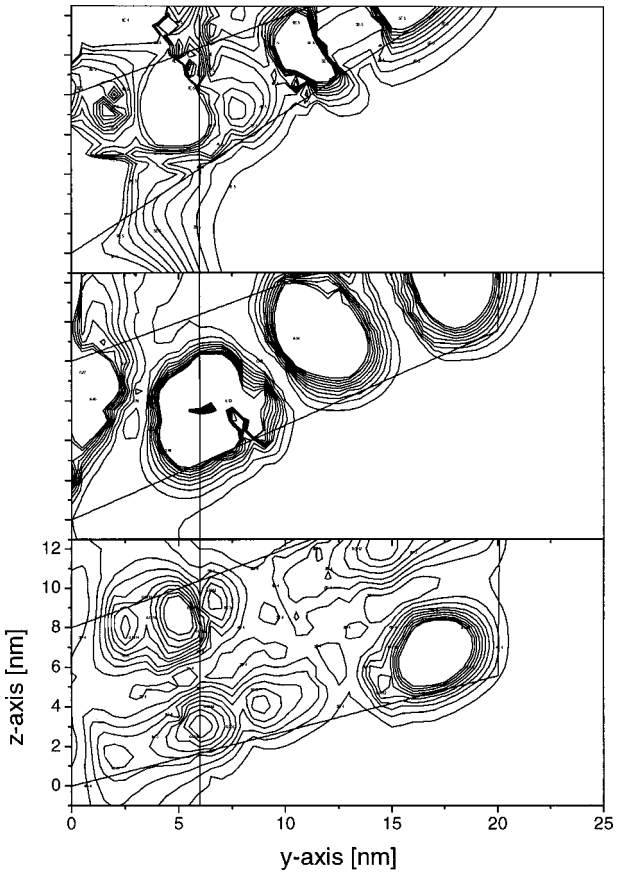

FIG. 5. Same as Fig. 4 but for the ground state in the VQWL region. $E=0.199$ eV.

$$\boldsymbol{A}=A_x\boldsymbol{x}_0+A_y\boldsymbol{y}_0, \tag{4}$$

here $\boldsymbol{p}$ is the crystal momentum, $\boldsymbol{x}_0$ and $\boldsymbol{y}_0$ are unit vectors in the x and y directions. It is easy to show that

$$\langle\Psi_{n,k}(\boldsymbol{r})|\boldsymbol{A}\cdot\boldsymbol{p}|\Psi_{m,q}(\boldsymbol{r})\rangle=\delta_{k,q}A_y\langle\psi_n(y,z)|p_z|\psi_m(y,z)\rangle \tag{5}$$

so that the averaged transition probability per unit time is

$$\left|\frac{eA_y}{m^*}\langle\psi_n(y,z)|p_z|\psi_m(y,z)\rangle\right|^2\frac{2\Gamma}{(E_n-E_m-\hbar\omega)^2+\Gamma^2}, \tag{6}$$

where E_n and E_m are eigenvalues of sublevel n and m, respectively. Γ is the relaxation energy of the excited states. $\hbar\omega$ is the energy of the incident radiation.

For nonpolarized incident radiation

$$|\langle A_x\rangle|^2=|\langle A_y\rangle|^2=\frac{|\langle\boldsymbol{A}\rangle|^2}{2}, \tag{7}$$

$|\langle\boldsymbol{A}\rangle|^2$ is proportional to the photon density, we finally obtain the optical absorption coefficient of the QWR system

$$\alpha_{nm}(\hbar\omega)=\frac{\Gamma|\langle\psi_n(y,z)|p_z|\psi_m(y,z)\rangle|^2}{(E_n-E_m-\hbar\omega)^2+\Gamma^2} \tag{8}$$

apart from physical constants.

By the spatial distributions of the two-dimensional wave functions we are able to calculate the absorption spectrum from the earlier expression. The results are presented in Fig. 6. It is observed here that due to the effective quantum confinement from the two (111)-surfaces, the optical matrix element between QWR and VQWL ground states is very small, so is the absorption coefficient.

Again, we consider the artificial reduction of the quantum confinement from the V groove. The amplitude of the two-dimensional wave function at 0.199 eV (band edge of the continuous states in the VQWL) is plotted in Fig. 5 as a function of θ. By reducing the quantum confinement effect we can significantly increase the overlapping of the two ground states so that the matrix element and the absorption

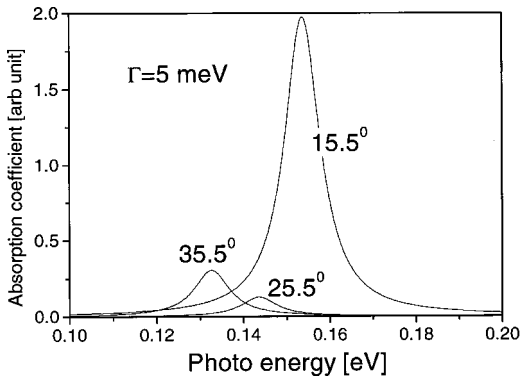

FIG. 6. Absorption coefficient as a function of the quantum confinement. $\Gamma=5$ meV.

coefficient increase greatly. However, the process is not linear as demonstrated by Fig. 6 since we have to take into account the optical coupling along the z direction in addition the wave function overlapping along the y direction [Eq. (8)].

The wave function $\psi_{0.199}(y,z)$ is rather complicated in the region where the VWQL crosses with the QWR. Wave function resonance is observed in the quantum wire region. The resonance is rather chaotic for the case of $\theta=35.5°$. However, within the spatial region of significant $\psi_{0.066}$, $\psi_{0.199}$ reaches its positive maximal at about $z=7$ nm and negative maximal at $z=2$ and 10 nm. Optical transition is thus allowed along the z direction but the matrix element of p_z is very small due to the small overlapping between the two wave functions along the y axis. The experimental result of rather weak photocurrent signal (Fig. 2) is thus understood from this basic optical transition point of view. The weak photocurrent can also be a result of small spatial area of the QWR as compared with the SQWL and PQWL layers.

For $\theta=25.5°$ and $15.5°$, $\psi_{0.199}(y,z)$ has clearly resonances in the QWR region. Numerically and approximately along the y axis, and within the region of significant $\psi_{0.055}$ at $\theta=25.5°$ (see Fig. 5)

$$\begin{aligned}\psi_{0.055}(y,z)&\approx\sin\left(\frac{\pi z}{L}\right)e^{-0.1y},\\ \psi_{0.199}(y,z)&\approx\sin\left(\frac{\pi z}{L}\right)\sin(0.1\pi y),\end{aligned}\tag{9}$$

when y is in the unit of nanometers. For the case of $\theta=15.5°$,

$$\begin{aligned}\psi_{0.045}(y,z)&\approx\sin\left(\frac{\pi z}{L}\right)e^{-0.05y},\\ \psi_{0.199}(y,z)&\approx\sin\left(\frac{2\pi z}{L}\right)\sin[0.12\pi(y-2)].\end{aligned}\tag{10}$$

It can thus be observed here that the overlapping along the y axis between the ground state in the QWR and $\psi_{0.199}$ increases with decreasing θ, mainly due to the spatial expansion of the QWR ground state (comparing Fig. 4 with Fig. 5). However, the matrix element of p_z along the z direction is minimized when $\theta=25.5°$ as the two wave functions have almost the same spatial variations along the z axis. The total optical transition rate and therefore the absorption coefficient are much reduced due to the forbidden transition. The absorption coefficient in this case is even lower than the one of our original V-grooved QWR.

The best optical transition is obtained when $\theta=15.5°$ where the spatial oscillation frequency of $\psi_{0.199}$ is twice the one of the ground state in the QWR region [Eqs. (10)], resulting in a maximal matrix element along the z direction, while on the other hand the overlapping of the two wave functions along the y axis is also optimal. The resulting absorption coefficient is increased by a factor of 4 when compared with the original V-grooved QWR (Fig. 6).

IV. SUMMARY

In a brief summary we have fabricated and characterized $GaAs/Al_{0.5}Ga_{0.5}As$ V-grooved quantum-wire-based infrared photodetectors. Theoretically we have discovered that the spatial extension of the QWR ground state is rather narrow due to the effective quantum confinement from the two (111)-surfaces which form the V groove. The spatial overlapping between the QWR ground state and the ground state in the VQWL region is small resulting in a small optical transition matrix element and a weak absorption coefficient. The photocurrent density is therefore rather weak, which contributes as the first cause of the weak photocurrent signal demonstrated experimentally.

Different quantum confinement structures in the QWR photodetector (SQWL, VQWL, and PQWL) further complicate the analysis and understanding of the system. Coulomb potential induced by the doped donors and redistributions of free carriers in different confinement structures, carrier transport processes among different confinement structures, the dark and photocurrents induced by the external bias are just a few examples for further theoretical and experimental investigations.

In the present work we concentrate on the intrinsic optical coupling between carriers confined in the quantum wire region and the external infrared radiation. It has been shown that when the incident radiation propagates along the z direction and the quantum wires are aligned along the x direction, the optical transition of the two-dimensional QWR system of Fig. 1(b) is determined by two factors, the optical coupling along the z direction and wave function overlapping along the y direction. QWR infrared photodetector optimization and design become thus difficult. It is much more complicated than the design of quantum well infrared photodetector due to the complication of the two-dimensional quantum confinement. The spatial distribution of the ground state in the QWR region is normally well behaved. Due to the spatial variation of the well width and well depth, the control over the excited states is, however, difficult.

[1] L. Esaki and R. Tsu, IBM J. Res. Dev. **14**, 61 (1970).
[2] R. Tsu and L. Esaki, Appl. Phys. Lett. **19**, 246 (1971).
[3] R. Tsu and L. Esaki, Appl. Phys. Lett. **22**, 562 (1973).
[4] S. D. Gunapala, *et al.*, IEEE Trans. Electron Devices **45**, 1890 (1998).
[5] J. P. Sun, G. I. Haddad, P. Mazumder, and J. N. Schulman, Proc. IEEE **86**, 641 (1998).
[6] H. Sakaki, Jpn. J. Appl. Phys., Part 2 **19**, L735 (1980); Y. Arakawa and H. Sakaki, Appl. Phys. Lett. **40**, 939 (1982).
[7] *Epitaxial Microstructures, Semiconductor and Semimetals*, edited by A. C. Gossard (Academic, San Diego, 1994), Vol. 40.
[8] A. Yariv, Appl. Phys. Lett. **53**, 1033 (1988).
[9] S. Tiwari and J. M. Woodall, Appl. Phys. Lett. **64**, 2211 (1994).
[10] S. Watanabe, S. Koshiba, M. Yoshita, H. Sakaki, M. Baba, and H. Akiyama, Appl. Phys. Lett. **75**, 2190 (1999).
[11] T. Sugaya, T. Takahashi, T. Nakagawa, M. Ogura, and Y. Sugiyama, J. Cryst. Growth **201–202**, 833 (1999).
[12] Y.-Q. Wang, Q. Huang, and J.-M. Zhou, Appl. Phys. Lett. **74**, 1412 (1999).
[13] D. Kaufman, Y. Berk, B. Dwir, A. Rudra, A. Palevski, and E. Kapon, Phys. Rev. B **59**, 10433 (1999).
[14] X.-Q. Liu *et al.*, Appl. Phys. Lett. **75**, 3339 (1999).
[15] J. Wu, B. Xu, X. Li, Q. W. Mo, Z. G. Wang, X. M. Zhao, and D. Wu, J. Cryst. Growth **197**, 95 (1999).
[16] A. Passaseo, M. Longo, R. Rinaldi, R. Cingolani, M. Catalano, A. Taurino, and L. Vasanelli, J. Cryst. Growth **197**, 777 (1999).
[17] G. Y. Slepyan, S. A. Maksimenko, V. P. Kalosha, J. Herrmann, N. N. Ledentsov, I. L. Krestnikov, Z. I. Alferov, and D. T. I. Bimberg, Phys. Rev. B **59**, 12275 (1999).
[18] W. Heiss *et al.*, Appl. Phys. Lett. **75**, 974 (1999).

[19] C. Teichert, J. C. Bean, and M. G. Lagally, Appl. Phys. A: Mater. Sci. Process. **67**, 675 (1998).
[20] A. Saar, S. Calderon, A. Givant, O. Ben-Shalom, E. Kapon, and C. Caneau, Phys. Rev. B **54**, 2675 (1996).
[21] R. Rinaldi, P. V. Giugno, R. Cingolani, F. Rossi, E. Molinari, U. Marti, and F. K. Reinhart, Phys. Rev. B **53**, 13710 (1996).
[22] T. Inoshita and H. Sakaki, J. Appl. Phys. **79**, 269 (1996).
[23] G. Creci and G. Weber, Semicond. Sci. Technol. **14**, 690 (1999).
[24] X.-Q. Liu *et al.* (unpublished).
[25] Y. Fu and M. Willander, *Physical Models of Semiconductor Quantum Devices* (Kluwer, Dordrecht, 1999), pp. 233–254, Chap. 6.
[26] Y. Fu, M. Willander, E. L. Ivchenko, and A. A. Kiselev, Phys. Rev. B **47**, 13498 (1993).